Molybdenum-oxysulfide Functionalized MgAl Layered Double Hydroxides – A Sorbent for Selenium Oxoanions

Robiul Alam,[1] Subrata Chandra Roy, [1] Taohedul Islam, [1] Renfei Feng[2], Xianchun Zhu,[3] Carrie L. Donley,[4] Saiful M. Islam[1]*

[1]Department of Chemistry, Physics, and Atmospheric Sciences, Jackson State University, Jackson, Mississippi 39217, United States

[2]Canadian Light Source, Saskatoon, Saskatchewan S7N 2V3, Canada

[3]Department of Civil Engineering, Jackson State University, Jackson, Mississippi 39217, United States

[4]Department of Chemistry, and Chapel Hill Analytical and Nanofabrication Laboratory (CHANL) University of North Carolina at Chapel Hill, North Carolina 27599, United States

ABSTRACT

Effective removal of chemically toxic selenium oxoanions at high-capacity and trace levels from contaminated water remains challenging in current scientific pursuits. Here, we report the functionalization of the MgAl layered double hydroxide with molybdenum-oxysulfide (MoO_2S_2) anion, referred to as LDH-MoO_2S_2, and its potential to sequester $Se^{VI}O_4^{2-}$ and $Se^{IV}O_3^{2-}$ from aqueous solution. LDH-MoO_2S_2 nanosheets were synthesized by ion-exchange method in solution. Synchrotron X-ray pair distribution function (PDF) and extended X-ray absorption fine structure (EXAFS) revealed an unexpected transformation of the $MoO_2S_2^{2-}$ to $[Mo_2O_2S_6]^{2-}$ like species during the intercalation process. LDH-MoO_2S_2 is remarkably efficient in removing SeO_4^{2-} and SeO_3^{2-} ions from ppm to trace level (≤10 ppb), with distribution constant (K_d) ranging from 10^4 to 10^5 mL/g. This material showed exceptionally high sorption capacities of 237 and 358 mg/g for SeO_4^{2-} and SeO_3^{2-}, respectively. Furthermore, LDH-MoO_2S_2 demonstrates a substantial affinity and efficiency to remove SeO_3^{2-}/SeO_4^{2-} even in the presence of competitive ions from

contaminated water. Hence, the removal of selenium (VI/IV) oxoanions collectively occurs through reductive precipitation and ion exchange mechanisms. This work provides significant insights into the chemical structure of MoO_2S_2 anion into LDH and emphasizes its exceptional potential for high-capacity selenium removal and positioning it as a premier sorbent for selenium oxoanions.

Keywords: layered double hydroxides, $MoO_2S_2^{2-}$, $Mo_2O_2S_6^{2-}$, wastewater purification, reductive precipitation, and ion exchange mechanisms.

TOC Graphic:

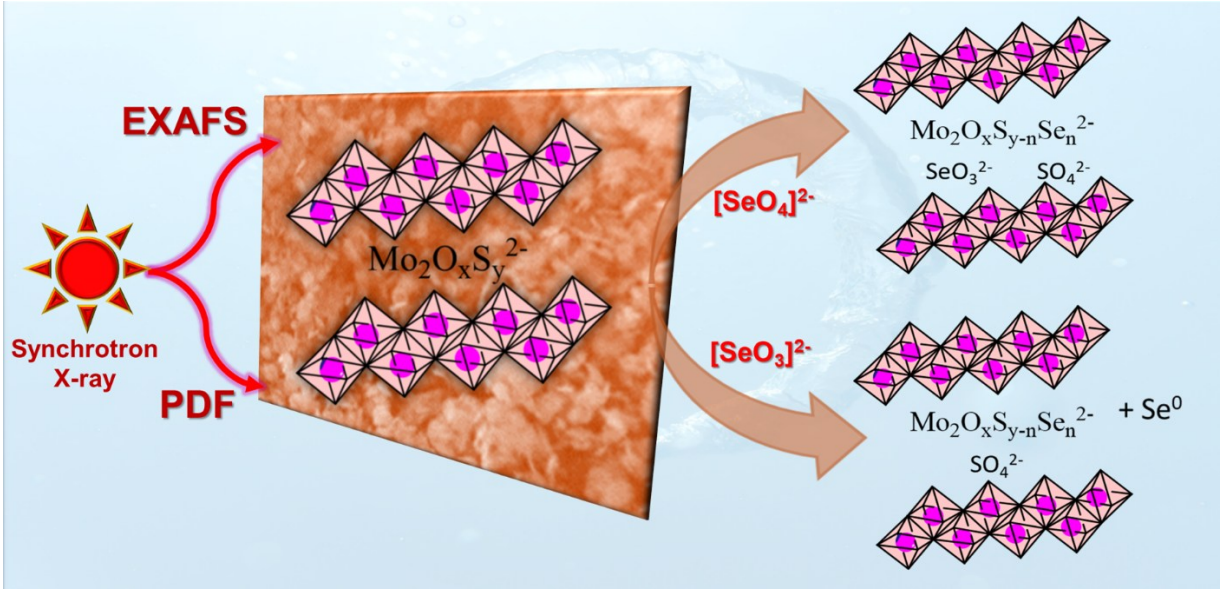

Synopsis: $MoO_2S_2^{2-}$ functionalized LDH nanosheets exhibit unpredictable structural transformation from $MoO_2S_2^{2-}$ to $Mo_2O_2S_6^{2-}$ like species during the intercalation process, enabling a high-capacity removal of selenium oxoanions, followed by reductive precipitation and ion exchange mechanisms.

INTRODUCTION

Selenium at trace levels is important for the correct functioning of both humans and animals as it plays an integral part in various physiological processes, but in high amounts, it may impose serious health problems.[1–3] Moreover, because of its chemical and radiological toxicity selenium can cause severe environmental problems globally.[4,5] Therefore, governments of different countries have enacted stringent selenium control regulations.[6]

Selenium enters into the environment both by natural and human-related pathways. Natural sources of selenium emissions arise from the erosion and weathering of substrates that contain high-levels of selenium, such as phosphatic rocks and coal deposits.[7] On the other hand, human-related contributions to selenium contamination are mainly linked to industrial activities, such as mining operations and the burning of fossil fuels.[8] These activities enable the deposition of selenium into the atmosphere and its subsequent leaching into the aquatic environment.[9] In aquatic systems, selenium mainly remains as soluble oxoanions, such as selenate ($Se^{VI}O_4^{2-}$) and selenite ($Se^{IV}O_3^{2-}$), and is important to remove for the safeguard of biological systems.

Several materials, including metal-organic frameworks[10], titanate nanotubes[11], carbon nanotubes[12], magnesium oxide[13], alumina oxide[14], titanium oxide[15], and numerous other metal oxides[16] have demonstrated functionalities in removing selenium from water. Despite the discovery of such diverse materials, the removal of selenium oxoanions, specifically $Se^{IV}O_3^{2-}$ and $Se^{VI}O_4^{2-}$, at trace-levels poses significant challenges due to numerous factors, including chemical stability, high solubility in water, competition for sorption sites, limitations in kinetics, complexation with other ions, and the technological limitations of existing remediation methods.[7,17–20]

Layered double hydroxides (LDHs) are two dimensional (2D) anionic clay, represented by the formula $[M^{2+}_{1-x}M^{3+}_{x}(OH)_2]^{x+}(A^{n-})_{x/n}\cdot mH_2O$, where M and A denote metals and anions, respectively.[21–25] The intriguing structure of LDH incorporates versatile sorption mechanisms, including surface adsorption, interlayer anion exchange, and the reconstruction of LDH layers, enabling the removal of chemically diverse oxoanions from wastewater.[7,22,26–28] However, without functionalization LDH suffers low specificity and adsorption capability for oxoanionsic species of selenium. Previously, we reported metal-sulfide intercalated LDH, as referred to LDH-MoS_4, as effective sorbent for toxic oxoanions of Se(IV), and Se(VI).[29] This finding underscores the importance of functionalizing LDH with chemically diverse thioanionic species and determine their effectiveness in the removing of selenium oxoanions from aqueous solutions.

In this work, we report the pioneering synthesis of a metal-oxysulfide intercalated LDH, referred to as LDH-MoO_2S_2. With synchrotron X-ray pair distribution function (PDF) and extended X-ray absorption fine structure (EXAFS), we unveiled the structural transformation of the molecular $MoO_2S_2^{2-}$ to $Mo_2O_2S_6^{2-}$ like species during the intercalation of $MoO_2S_2^{2-}$ into LDH-NO_3. We further show its effectiveness in removing selenium oxoanions of $Se^{VI}O_4^{2-}$ and $Se^{IV}O_3^{2-}$ from ppm level to the trace-level, ≤10 ppb with a K_d value of $\geq 10^4$ mL/g. We also demonstrate that LDH-MoO_2S_2 displays noteworthy adsorption capacities of 237 mg/g for SeO_4^{2-} and 358 mg/g for SeO_3^{2-} and effectively removing them from highly contaminated water. These results showcase a superior potential of LDH-MoO_2S_2 for the highly efficient removal of selenium from contaminated water.

EXPERIMENTAL SECTION

LDH Preparation: The MgAl-LDH-CO_3 (LDH-CO_3) was synthesized according to procedures described in previous work.[24] The MgAl-LDH-NO_3 (LDH-NO_3) was obtained by ion exchange of the CO_3^{2-} ion, described in details the supporting information file (SI). The intercalation of $MoO_2S_2^{2-}$ anion into LDH-NO_3 was conducted by anion exchange. In detail, for the synthesis of MgAl-LDH-MoO_2S_2, 0.3 g of MgAl-LDH-NO_3 and 0.3 g of $(NH_4)_2MoO_2S_2$ were dispersed in 10 mL formamide**.** The mixture was then stirred at ambient conditions for 24 h leading to the formation of orange solutions with suspended particles. After the filtration, orange solids were obtained, washed with ethanol, and dried under ambient conditions. The synthesis of $(NH_4)_2MoO_2S_2$ was conducted following the procedure outlined in a prior study.[30] A detail on the synthesis is reported in the SI.

Adsorption Experiments: The adsorption experiments of $Se^{IV}O_3^{2-}$ and $Se^{VI}O_4^{2-}$ oxoanions by the LDH-MoO_2S_2 were performed at room temperature (RT). Details on the sorption experiments, investigations of sorption isotherms, kinetics, and removal efficiencies for selenium(IV/VI) oxoanions are reported in the SI.

Characterization: Samples were analyzed by X-ray powder diffraction (XRD), scanning electron microscopy (SEM), transmission electron microscopy (TEM), energy dispersive spectroscopy (EDS), infrared (FT-IR) spectroscopy, Raman spectroscopy, X-ray photoelectron spectroscopy (XPS), inductively charged coupled mass spectroscopy (ICP-MS), **s**ynchrotron X-ray pair distribution function (PDF), and extended X-ray absorption fine structure (EXAFS), please see detains in the SI.

RESULTS AND DISCUSSION

Synthesis and characterizations of LDH-MoO_2S_2: The LDH-CO_3 was synthesized by a hydrothermal synthesis; subsequently, the nitrate and molybdenum oxysulfide (MoO_2S_2) anions were intercalated into the positively charged lamellar of the LDH by a stepwise ion-exchange reaction: LDH-CO_3 → LDH-NO_3 → LDH-MoO_2S_2 to produce the MoO_2S_2 functionalized ultrathin LDH (Schematic 1). X-ray powder diffraction revealed the shift in the characteristic d_{003} peak position of LDH-CO_3, LDH-NO_3, and LDH-MoO_2S_2 from 0.76 → 0.89 →1.05 nm (Figure 1a) that matches the previously reported XRD pattern of the CO_3^{2-} to NO_3^- ion exchange.[24,31,32] This change in the d_{003} peak position corresponds to the increase of the basal space due to the accommodation of the larger anions of NO_3^- and $MoO_2S_2^{2-}$ in the interlayer space of the LDH. It is noteworthy that after the intercalation, the (003) reflection at 1.05 nm significantly weakens as compared to the (006) reflection at 0.53 nm. In agreement with Ma *et al*., we believe that the intercalation of the heavy $(MoO_2S_2)^{2-}$ anions and their strong scattering characteristic leads to this phenomenon.[32] Infrared spectrum (IR) showing the strong band centering at about 1358 cm^{-1} for the CO_3^{2-} intercalated LDH; however, after the nitrate intercalation peak position remains same but their shape becomes distinctive (Figure 1b).[24,33,34] This further demonstrates the incorporation of nitrate anion, however, the presence of CO_3^{2-} along with NO_3^- can't be ignored. This peak was almost abolished for the LDH-MoO_2S_2 (Figure 1b), which suggests the exchange of the NO_3^- anion by the $[MoO_2S_2]^{2-}$ species. Hence the intercalation of was achieved using a large excess of $[MoO_2S_2]^{2-}$ as specified in the experimental section.

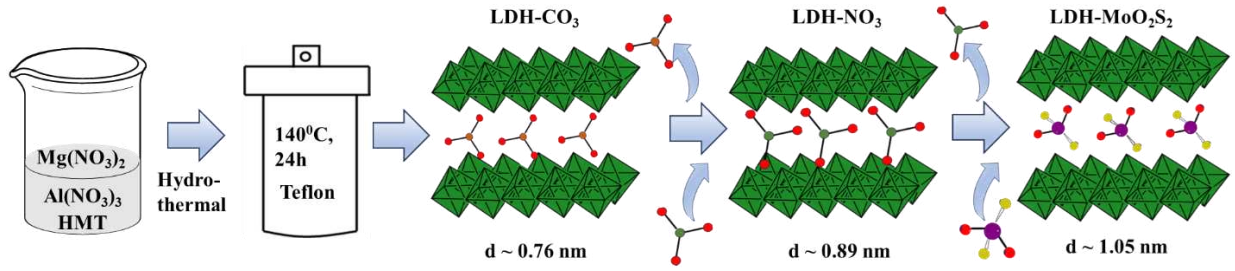

Schematic 1: A schematic diagram of the synthesis of LDH-CO_3, followed by ion exchange of CO_3^{2-} with the NO_3^- anions for the synthesis of LDH-NO_3; subsequently by $MoO_2S_2^{2-}$ anions to synthesize the $MoO_2S_2^{2-}$ intercalated LDH-MoO_2S_2.

The morphology of the LDH-NO_3 and LDH-MoO_2S_2 were examined by using scanning electron microscopic (SEM) and transmission electron microscopy (TEM). SEM revealed that both the NO_3 and the $MoO_2S_2^{2-}$ intercalated LDHs retained a hexagonal plate-like morphology (Figure S2). The ultrathin hexagonal sheets of LDH are visible in TEM (Figure 1c). Elemental mapping of the LDH-MoO_2S_2 shows the presence and the homogeneous distribution of Mg, Al, Mo, and S (Figure S3). Energy dispersive X-ray spectroscopy (EDS) analysis of LDH-MoO_2S_2 revealed an average atomic abundance of 35.04, 22.94,12.40 and 29.62 % for Mg, Al, Mo, and S atoms, respectively (Figure S2). This finding further demonstrates the successful introduction of $MoO_2S_2^{2-}$ species into the interlayer of MgAl-LDH. Note that oxygen was not determined by EDS due to the unreliability of its quantitative determination. Solid-state UV/vis absorption spectroscopy of the crystalline orange powder of LDH-MoO_2S_2 revealed a band gap energy of ~2.04 eV (figure S4). This finding suggests that the LDH-MoO_2S_2 is a medium band gap semiconductor.

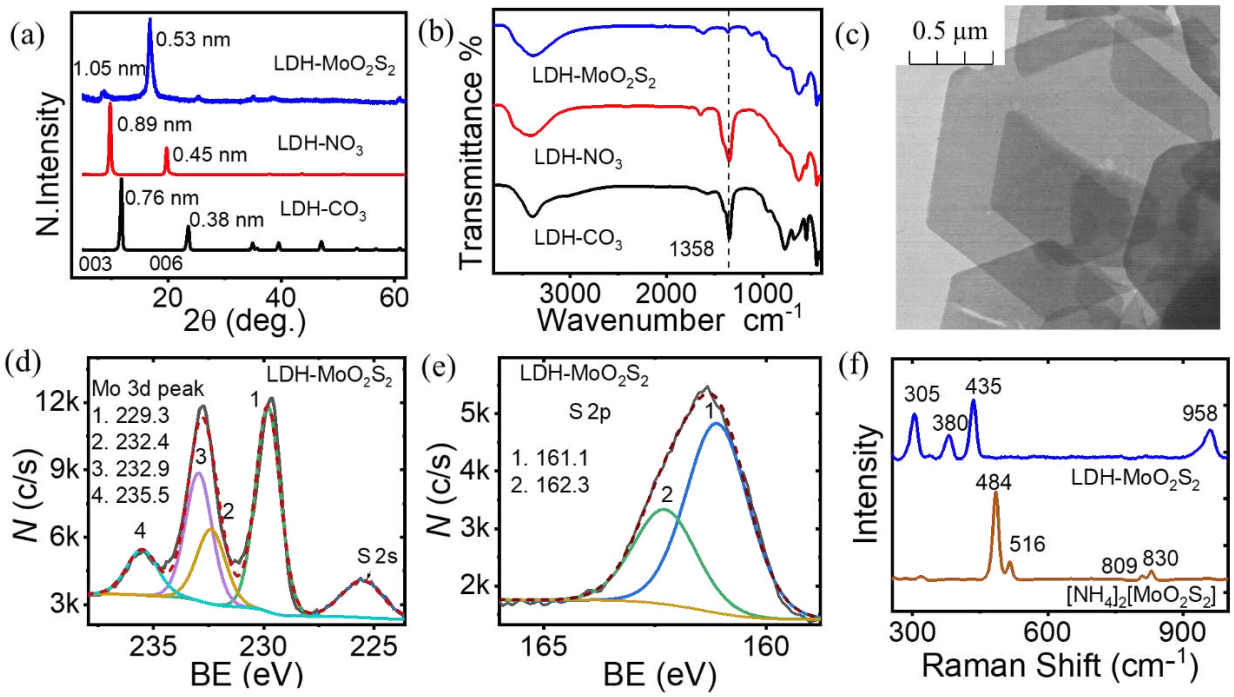

Figure 1. Comparison of XRD patterns (a), FT-IR spectra (b) of LDH-CO_3, LDH-NO_3, and LDH-MoO_2S_2; TEM image of the LDH-MoO_2S_2 showing the hexagonal morphology (c); XPS spectra of LDH-MoO_2S_2 with the deconvolution of associated XPS peaks: Mo 3d (d), and S 2p (e); and Raman spectra of $(NH_4)_2MoO_2S_2$ and LDH-MoO_2S_2 (f).

XPS analysis of the LDH-MoO_2S_2 (Figure 1 d, e) revealed the chemical state of Mo and S. The binding energies (BEs) at 232.4 and 235.5 eV (Figure 1d) were assigned $3d_{5/2}$ and $3d_{3/2}$, respectively of Mo^{6+}.[35–41] Besides the Mo^{6+} peaks, there exists a pair of peaks at 229.3 and 232.9 eV, for Mo 3d orbital energies. Importantly, for the precursor $(NH_4)_2MoO_2S_2$ the intense peaks at 233.69eV, 230.51 eV are attributed to Mo 3d orbital energy (Figure S5). Hence such a difference in the BEs between the precursor and LDH-MoO_2S_2 suggests a change in the electronic structure and/ coordination environment of Mo atoms after the intercalation or a change in coordination environment of Mo atoms after the intercalation, which is not clear to us. Besides, XPS of LDH-MoO_2S_2 shows strong bands at 161.1 and 162.3 eV, which correspond to the BEs of S 2p for S^{2-}.[35,42] Raman spectrum shows strong peaks ranging from 300 - 440 cm^{-1}, which are related to Mo-S modes.[35,36,43] Besides, Raman spectrum of the $(NH_4)_2MoO_2S_2$ (Figure 1f) revealed two

distinguish peaks at 809 and 830 cm^{-1} that correspond to ν(Mo-O),[30,35,43,44] whereas after intercalation, LDH-MoO_2S_2 shows a strong bands centered at 958 cm^{-1} suggesting the presence of Mo=O bond.[35,36,45] This peak was notably absent in the Raman spectrum of the precursor materials, reflecting a significant structural transformation during the ion exchange process.

To understand the structural insights of the interlayered anion of LDH-MoO_2S_2, we conducted a comprehensive analysis, including synchrotron X-ray pair distribution function (PDF) and extended X-ray absorption fine structure (EXAFS). These analyses suggest a transformation from the initial $MoO_2S_2^{2-}$ species to a $[Mo_2O_xS_y]^{2-}$ like structure. The Raman spectral feature at 958 cm^{-1} is interpreted as a direct manifestation of the Mo=O vibrational mode within the $[Mo_2O_xS_y]^{2-}$ like species, formed during the intercalation process.[46–49] Moreover, to assess the chemical states and bonding correlations in details, we analyzed the LDH-MoO_2S_2 by X-ray pair distribution function (PDF) and compared with LDH-NO_3 and $(NH_4)_2MoO_2S_2$ (Figure 2a). PDF of the $(NH_4)_2MoO_2S_2$ shows two strong correlations at ~1.78 and 2.19 Å. These peaks correspond to the Mo-O and Mo-S interactions as evidenced by the crystal structure of the $(NH_4)_2MoO_2S_2$.[44,46,50] Besides, the PDF of the LDH-NO_3 shows peaks at 1.83 Å (a shoulder) and 2.06 Å (strong), which can be assigned as Al-O and Mg-O bonding correlation, respectively.[51] In contrast, PDF of the LDH-MoO_2S_2 shows the absence of the peak at 2.19 Å that corresponds to Mo-S bonding correlation for the tetrahedral MoO_2S_2 anion. However, it shows the presence of a very strong peak at about 2.34 Å, which is consistent to Mo-S bonding correlation. Here, the increase of the Mo-S bond distance from 2.19 to 2.34 Å can be linked to an increase of the coordination number of Mo, which is due to the increase in the size of molybdenum ion. This could be attributed to the reduction of Mo^{6+} to a lower oxidation state followed a concurrent partial oxidation of some S^{2-}, which is not clear to us. However, a structural rearrangement driven change

in interatomic distance can't be completely ruled out." Moreover, a peak centered at about 1.80 Å could be the superimposed peak for Mo=O and Al-O, while the peak at about 2.84 may be attributed to the Mo-Mo correlation as observed in the $Mo_2O_2S_6^{2-}$ anions.[47]

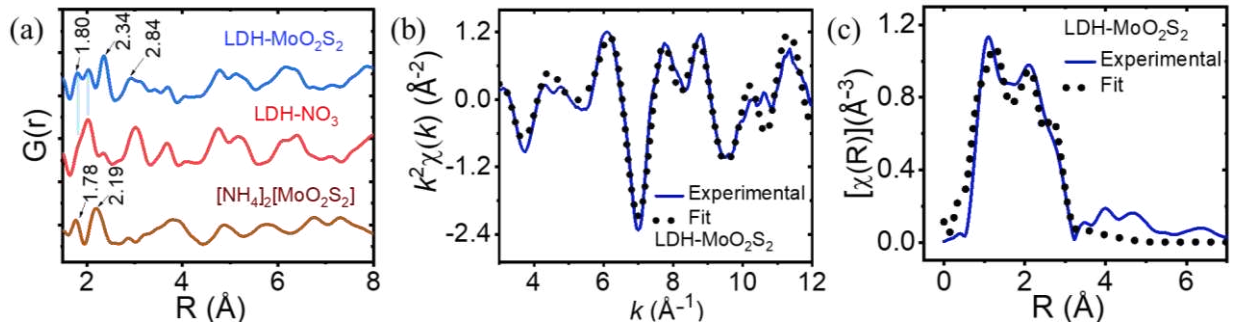

Figure 2: Synchrotron X-ray pair distribution function of $(NH_4)_2MoO_2S_2$, LDH-NO_3, and LDH-MoO_2S_2 (a); EXAFS of Mo-K-edge data for LDH-MoO_2S_2 (b), and its Fourier transforms (c).

The coordination environment of Mo was investigated using extended X-ray absorption fine structure (EXAFS) studies. Figure 2b and 2c represent the EXAFS data in k and R-space. Harnessing the structural entities obtained by PDF, XPS, and Raman, Mo K-edge EXAFS data was fitted by using multiple scattering paths, including Mo-Mo, Mo-S and Mo-O. Details on the results of the fitting are given Table S1. As expected from the PDF and XPS results, the fitting of the Mo K-edge was not converged straightforward to MoO_2S_2 anions alone, instated an additional compound, $(Me_4N)_2Mo_2O_2S_6$, was required to fit the data.[52] The fitting of the data yielded a $d_{(Mo–Mo)} \sim 2.92$ Å, which is close to the dimeric cluster of molybdenum, Mo_2 ($d_{(Mo–Mo)} = 2.83$ Å) of the $[Mo_2O_2S_6]^{2-}$.[47] Overall, the analysis of the Mo K-edge data revealed the presence of Mo-O, Mo-S, and Mo-Mo coordination environment. Hence, Mo-Mo bonding correlation can be attributed to the dimerization of the MoO_2S_2 ion. This kind of structural rearrangement is known for MoS_4^{2-} that undergoes dimeric rearrangement to $Mo_2S_7^{2-}$.[39] This finding suggests that the intercalation

chemistry of $MoO_2S_2^{2-}$ into LDH is remarkably complex, contrasting with the straightforward intercalation of the molecular precursors of metal-sulfides proposed previously for MoS_4^{2-}, $Mo_3S_{13}^{2-}$, SnS_4^{2-} and $Sn_2S_6^{2-}$ intercalated LDHs.[24,29,33,53–56]

Removal of $Se^{IV}O_3^{2-}$ and $Se^{VI}O_4^{2-}$ from water: The efficiency of LDH-MoO_2S_2 in removing SeO_4^{2-} and SeO_3^{2-} ions from aqueous solutions was investigated at neutral, acidic, and alkaline pHs (Figure S6). Our results suggest that LDH-MoO_2S_2 is more effective in removing $Se^{VI}O_4^{2-}$ at neutral pH than it is under acidic or alkaline conditions. At a neutral pH, LDH-MoO_2S_2 was able to remove about 99 % of $Se^{VI}O_4^{2-}$ (Table S2) from a 10^3 ppb spiked deionized water (DIW) solution leaving the final concentration of about 9 ppb with the K_d values of 8.2×10^4 mL/g. Hence, such a low residual concentration of the selenium is well below the US EPA's (50 ppb) and world health organization (WHO)'s tolerance limit (40 ppb).[29,57,58] Also, it is important to note that materials that possess K_d values $\geq10^4$ mL/g are commonly regarded as outstanding sorbents.[29,59,60] Hence, such a high K_d suggests that the sorbent LDH-MoO_2S_2 has a high affinity to sorbate, $Se^{VI}O_4^{2-}$ ions and thus could be useful for the decontamination of wastewater. The removal effectiveness of LDH-MoO_2S_2 for 10^4 ppb SeO_4^{2-} spiked deionized water solution shows 68.61% removal, whereas in acidic and alkaline conditions it shows only ~15% removal (Table S2).

On the other hand, LDH-MoO_2S_2 shows remarkably similar effectiveness in the removal of $Se^{IV}O_3^{2-}$ from acidic and pH neutral solutions. At neutral pH, LDH-MoO_2S_2 removed about 99.8% of SeO_3^{2-} from 10^3 ppb spiked DIW solutions and 97.7% from 10^4 ppb spiked DIW solutions (Table S3). At pH ~ 2, LDH-MoO_2S_2 can remove over 97.3% of SeO_3^{2-} from 10^3 ppb and 97.1% of SeO_3^{2-} from 10^4 ppb spiked solutions. LDH-MoO_2S_2 exhibited a K_d of ~ 4.5×10^5 mL/mg at neutral pH. It is noteworthy that LDH-MoO_2S_2 effectively captures SeO_3^{2-} ions, decreasing the concentration from 10^3 ppb to less than 10 ppb in neutral environments and less

than 30 ppb in acidic conditions. This finding suggests that LDH-MoO_2S_2 can efficiently remove selenium ion across a range of pHs, as demonstrated by its concertation reduction in neutral pH, which exceeds the US EPA limit for selenium by approximately five times, and the reduction in acidic conditions, which is about two times lower.[57,58] These results suggest that LDH-MoO_2S_2 could be a useful material for the removal of SeO_3^{2-} from water at acidic and neutral conditions. Control experiments involving LDH-NO_3 and $(NH_4)_2MoO_2S_2$ indicated that these materials exhibit lower efficacy in the sorption of selenate and selenite (Table S4). This finding underscores the importance of functionalizing LDH with MoO_2S_2 anions.

The kinetic studies of LDH-MoO_2S_2 for the removal of SeO_4^{2-} and SeO_3^{2-} were conducted using initial concentrations of 10^3 and 10^4 ppb of SeO_4^{2-} and SeO_3^{2-} in DIW over a period of ½ to 24 h of interactions at neutral conditions (Figure 3, Table S5-S8). In the initial 1-3 hours of interactions, LDH-MoO_2S_2 demonstrated a rapid and effective removal, achieving approximately 99 % removal for SeO_4^{2-} and SeO_3^{2-} (Table S5-S8) with K_d exceeding 10^5 mL/g for 10^3 ppb of Se(VI/IV) spike solutions. In contrast, for the 10^4 ppb spiked solutions the removal efficiency for SeO_4^{2-} and SeO_3^{2-} reaches over 95 and 99 %, respectively in 3 h. In general, two different rate equations, pseudo-first order and pseudo-second-order, are used to determine the sorption rates and properties.[33] A linear relationship is observed from the t/q_t versus t plots for both concentrations with a correlation factors of $R^2 \sim 1$ for SeO_4^{2-} and SeO_3^{2-}, respectively (Figure S7). The pseudo second-order rate constants were determined to be 2.835 g/mg·min^{-1} for 1.0×10^3 ppb of SeO_4^{2-} solutions and 15.189 g/mg·min^{-1} for 1.0×10^3 ppb of SeO_3^{2-} solutions, respectively (Table S9).

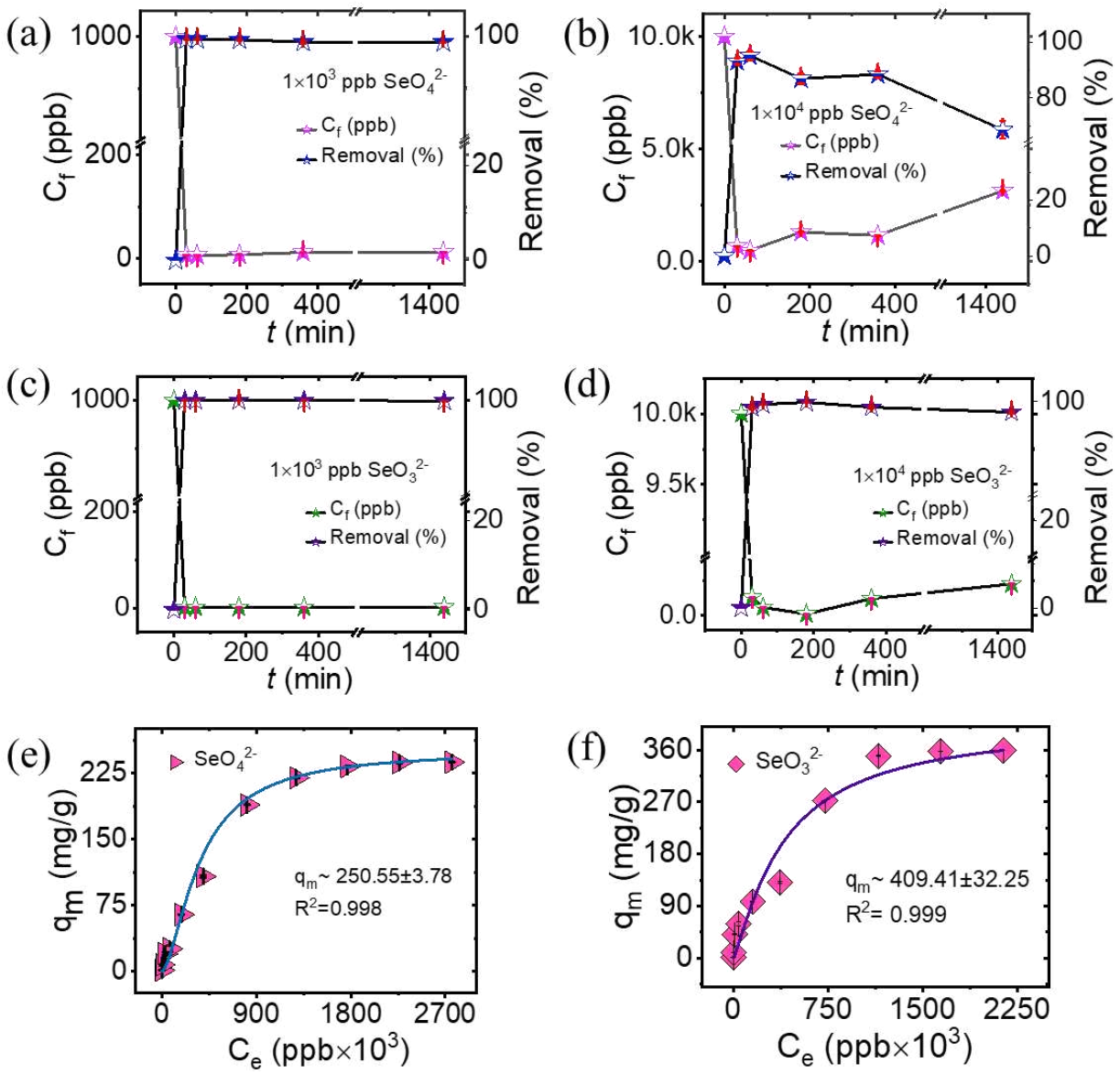

Figure 3: Time-dependent sorption experiment showing removal (%) of SeO_4^{2-} (a, b) and SeO_3^{2-} (c, d) by LDH-MoO_2S_2 spiked with 1×10^3 and 1×10^4 ppb of SeO_4^{2-} and SeO_3^{2-}; and adsorption capacity of SeO_4^{2-} (e) and SeO_3^{2-}(f).

To determine the uptake capacity of LDH-MoO_2S_2 towards SeO_4^{2-} and SeO_3^{2-}, we investigated the sorption of SeO_4^{2-} and SeO_3^{2-} for a broad range of concentrations (Table S10 and S11). This study reveals that the sorption capacity increases with the increase of SeO_4^{2-} and SeO_3^{2-} concentrations until it reaches an equilibrium. Figure 3e and 3f display the equilibrium sorption isotherms. For SeO_4^{2-}, LDH-MoO_2S_2 achieved a maximum sorption capacity of 237 mg/g. On the

other hand, the maximum sorption capacity of SeO_3^{2-} reaches 358 mg/g. The data points of Figures 3e and 3f were fitted to the Langmuir model, which revealed the calculated q_m values of 250.55 (±3.78) and 409.42 (±32.26) mg/g for SeO_4^{2-} and SeO_3^{2-}, respectively. These values of the calculated capacities are close to that of the experimental values. With such high capacities, LDH-MoO_2S_2 stands out as a highly efficient sorbent for both SeO_4^{2-} and SeO_3^{2-}, demonstrating a capacity comparable to the top candidates for selenate /selenite sorption, as shown in the Table 1.[10,22,26,29,61–65]

Table 1 Sorption capacities of various sorbents for selenate and selenite

Ions	Sorbents	q_m (mg/g)	Ref.
Se(VI)	**MgAl-MoO_2S_2-LDH**	**237**	**This work**
	FeMgAl-MoS_4-LDH	167	[22]
	MgAl-MoS_4-LDH	85	[29]
	NU-1000	62	[10]
	Fe^{2+} doped MgAl-LDH	110	[61]
	$Y_2(OH)_5Cl_{1.5}H_2O$	124	[62]
	CTFS-Cl	149	[63]
	JU-111	165	[64]
	GO/Al_{30} NC	156	[66]
	iMOF-3C	73	[67]
	Ca-Al-LDHs	139	[68]
Se(IV)	**MgAl-MoO_2S_2-LDH**	**358**	**This work**
	FeMgAl-MoS_4-LDH	484	[22]
	MgAl-MoS_4-LDH	297	[29]
	UPC-183-Eu	308	[65]
	JU-111	190	[64]

$Y_2(OH)_5Cl_{1.5}H_2O$	207	[62]
Mg/Al(Zn/Al)-LDH	119	[26]
nZVI/rGO	174	[69]

To determine the effectiveness of SeO_4^{2-} and SeO_3^{2-} removal in the presence of various competitive ions in purified and naturally contaminated water, we investigated selenium oxoanions removal efficiency from tap water and Mississippi River water (collected from Vidalia, Louisiana) by spiking with 1000 ppb of SeO_4^{2-} and SeO_3^{2-} (Figure S8, Table S12). This study showed that despite the presence of numerous ions, such as Ca^{2+}, Mg^{2+}, Na^+, K^+, HCO_3^-, SO_4^{2-}, and Cl^-, and other organic or inorganic constituents, LDH-MoO_2S_2 exhibits over ≥ 99 % removal efficiency for SeO_3^{2-}, while for SeO_4^{2-} it plunges to 33.7 and 27.5% for tap water and Mississippi river water, respectively. Hence, the difference in the removal efficiencies of SeO_4^{2-} and SeO_3^{2-} can be due to the competition from different anions found in tap and river water, which impact the selectivity of LDH-MoO_2S_2. Besides, LDH-MoO_2S_2 in general shows greater removal performance for SeO_3^{2-} than SeO_4^{2-}. This may be because the reduction of $Se^{IV}O_3^{2-}$ to Se^0/Se^{2-} is easier than $Se^{VI}O_4^{2-}$ for a Se^0/Se^{2-}chemical state, which is the dominant mechanism for the removal of these oxoanions, as explained later. This finding illustrates that LDH-MoO_2S_2 is highly capable in removing SeO_3^{2-} and moderately effective for SeO_4^{2-} separation from contaminated water.

Investigations of the SeO_3^{2-} and SeO_4^{2-} removal mechanisms: To understand the selenate and selenite sorption mechanisms, post interacted solid LDH-MoO_2S_2 was analyzed by SEM, EDS, XRD, and XPS. SEM image shows that the post interacted sample maintained its hexagonal morphology suggesting the retention of the layered type phases of LDH following the adsorption process (Figure S9). XRD revealed that the d_{003} spacing of the LDH expands to about

1.10 nm after interactions with both SeO_4^{2-} and SeO_3^{2-} (Figure 4a). This feature indicates an enlargement of the unit cell of the LDH along the crystallographic c-axis, which can be attributed due to the increased size of the interlayered anions. It is possible that selenium ion has replaced some sulfur in the $Mo_2O_xS_y^{2-}$ species. The bifurcates of the d_{006} peak in the XRD of post-interacted LDH may point to the presence of a weak unresolved peak in the broad tail of the d_{003} peak, which may be because of the phase segregation of the LDH structures, however, the formation of a secondary phase non-LDH phase can't be completely ruled out. Akin to EDS, XPS shows the presence of selenium in the post interacted samples (Figure S6 and Figure 4b). XPS of the $Se^{VI}O_4^{2-}$ interacted sample reveals strong bands at about 58.80 and 59.65 eV. These values correspond to $3d_{5/2}$ and $3d_{3/2}$ orbital energy of Se^{4+}.[29,42,70,71] In addition, XPS also shows a broad band centering at about 54.5 eV. The deconvolution of this peak revealed two peaks. The peaks at about 54.10 and 54.95 eV can be attributed to $3d_{5/2}$ and $3d_{3/2}$ orbital energy of the selenide (Se^{2-}).[70–72] This finding suggests that during the interaction of SeO_4^{2-} with LDH-MoO_2S_2, $Se^{VI}O_4^{2-}$ is reduced to several oxidation states, Se^{4+} and Se^{2-}.[70,72] In contrast, SeO_3^{2-} interacted LDH-MoO_2S_2 revealed a broad photoelectron spectrum in the range of 53 to 57 eV. The deconvolution of this spectrum revealed four bands having maxima at ~ 54.14, 54.95, 55.00 and 55.82 eV (Figure 4c). These values of the binding energies are related Se^0 and Se^{2-} oxidation states, respectively.[70–72] This finding proves that SeO_4^{2-} and SeO_3^{2-} were reduced throughout the sorption process. However, the presence of the Se(IV) ions in the $Se^{VI}O_4^{2-}$ interacted LDH-MoO_2S_2 is indicative of the presence of $Se^{IV}O_3^{2-}$ like species.

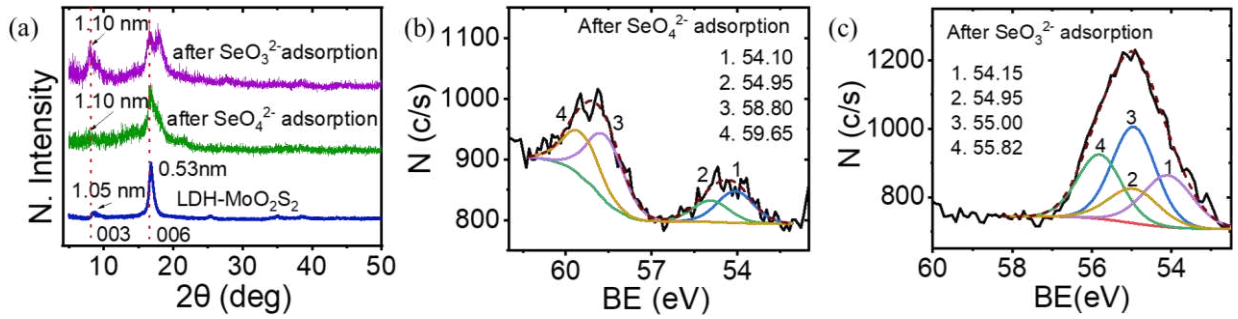

Figure 4: XRD patterns of pre- and post- SeO_4^{2-} and SeO_3^{2-} adsorbed LDH-MoO_2S_2 (a), XPS spectra showing Se 3d peaks after adsorption of SeO_4^{2-} (b) and SeO_3^{2-} (c).

Overall, analysis of the post-interacted LDH-MoO_2S_2 suggests that an intricate process, including reduction and ion-exchange, is involved in the removal of selenate and selenite from water, as shown in the schematic (Figure 5). An interaction between the $Se^{VI}O_4^{2-}$ and LDH-MoO_2S_2 leads to the formation of Se^{4+} and Se^{2-}, while for $Se^{IV}O_3^{2-}$ it results in Se^0 and Se^{2-} (Figure S7, Table S13). Besides, the presence of the Se^{2-} anions in the post interacted samples could be attributed to the substitution of sulfide from the interlayered anions of $Mo_2O_xS_y$ to $Mo_2O_xS_{y-n}Se_n$. The substitution of the S^{2-} by Se^{2-} could be linked to the increase in the interlayered distance from 1.05 to 1.10 nm from the pristine to post-interacted LDH (Figures 4a). Also, the formation of the Se^{4+} ions after the interaction of the $Se^{VI}O_4^{2-}$ may result in the formation of the $HSe^{IV}O_3^-/Se^{IV}O_3^{2-}$, settling in the interlayer of LDH, followed by a partial substitution of the molybdenum oxysulfides. Hence, the reduction of selenium of $Se^{VI}O_4^{2-} \rightarrow Se^{IV}O_3^{2-} \rightarrow Se^0/Se^{2-}$ can be attributed to the concurrent oxidation of some sulfides to sulfates. which remain inside the LDH structure as indicated by XPS of post adsorbent materials (Figure S10, Table S13). During the process, some Mo leaches into solution which may remain as MoO_4^{2-} or $MoO_xS_{4-x}^{2-}$ ions.[32]

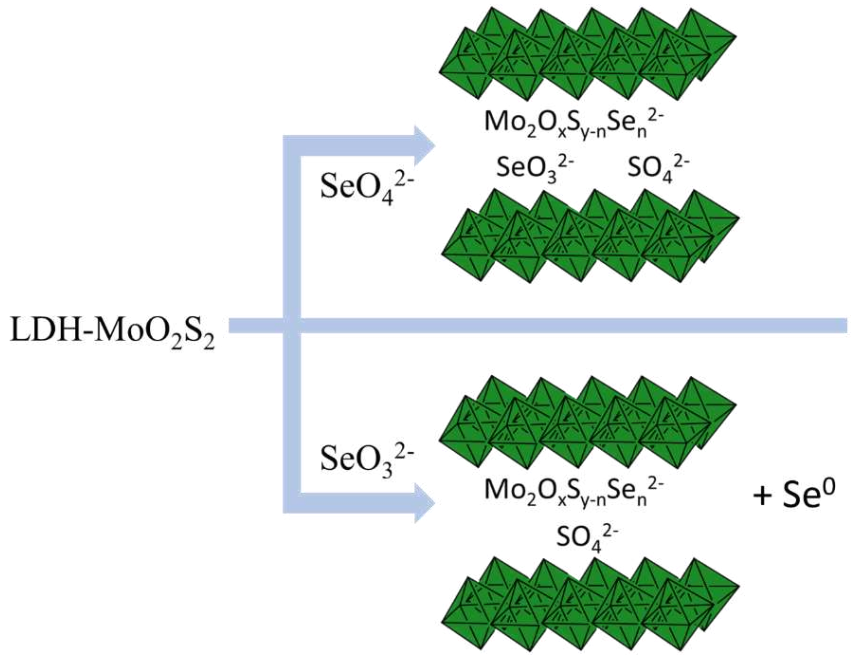

Figure 5: Schematic shows a plausible sorption mechanism of SeO_4^{2-} and SeO_3^{2-} ions by LDH-MoO_2S_2.

Finally, this work showcases the functionalization of MgAl layered double hydroxide with $MoO_2S_2^{2-}$, reveals the transformation of the interlayered anions, and evaluates its effectiveness in removing selenium oxoanions from water. Importantly, the structural rearrangement of the $MoO_2S_2^{2-}$ anions during the intercalation process into the MgAl-LDH emphasizes the importance of investigating the chemical fate of the metal-sulfide species after the intercalation into LDH layers ─ a phenomenon overlooked in previous studies on MoS_4^{2-}, $Mo_3S_{13}^{2-}$, SnS_4^{2-} and $Sn_2S_6^{2-}$ intercalated LDHs.[24,29,33,53–56] Apart from this, the potential of the $MoO_2S_2^{2-}$ functionalized LDH for exceedingly high-capacity and trace-level selenium removal underscores the significance of LDHs' functionalization with versatile metal-oxysulfide, and -sulfide anions of diverse chemical compositions, and uncovering their effectiveness for the removal of selenium oxoanions from contaminated water systems.

ACKNOWLEDGEMENT

This work was supported by the National Science Foundation (NSF) Division of Chemistry (NSF-2100790). RA is also thankful to the US Department of Energy Minority Serving Institution Partnership Program (MSIPP) managed by the Savannah River National Laboratory under SRNS contract (RFP No.0000542525 and 0000458357). TI acknowledges US Department of Energy's Building EPSCoR-State/National Laboratory Partnerships DE-FOA-0002624. This work was performed in part at the Chapel Hill Analytical and Nanofabrication Laboratory, CHANL, a member of the North Carolina Research Triangle Nanotechnology Network, RTNN, which is supported by the National Science Foundation, Grant ECCS-2025064, as part of the National Nanotechnology Coordinated Infrastructure, NNCI. A portion of this work was performed using XPS/UPS/IPES instrumentation supported by the Center for Hybrid Approaches in Solar Energy to Liquid Fuels (CHASE), an Energy Innovation Hub funded by the U.S. Department of Energy, Office of Science, Office of Basic Energy Sciences under Award Number DE-SC0021173. This research used resources of the Advanced Photon Source; a U.S. Department of Energy (DOE) Office of Science User Facility operated for the DOE Office of Science by Argonne National Laboratory under Contract No. DE-AC02-06CH11357. The mail-in program at Beamline 11-ID-B (and/or 17-BM, 11-BM) contributed to the data. X-ray absorption spectroscopy measurements were performed at the VESPERS, Canadian Light Source, which is supported by the Canada Foundation for Innovation (CFI), the Natural Sciences and Engineering Research Council (NSERC), the National Research Council (NRC), the Canadian Institutes of Health Research (CIHR), the Government of Saskatchewan, and the University of Saskatchewan. Any use of trade, firm, or product names is for descriptive purposes only and does not imply endorsement by the U.S. Government.

Corresponding Author:

Saiful M. Islam - Department of Chemistry, Physics, and Atmospheric Sciences, Jackson State University, Jackson, Mississippi 39217, United States; Orcid: https://orcid.org/0000-0001-8518-1856; Email: muhammad.s.islam@jsums.edu

Orchid: http://orcid.org/0000-0001-8518-1856

Author Contributions:

This manuscript was written through the contributions of all authors. All authors have given approval to the final version of the manuscript.

Associated Content

Supporting Information Available:

Synthesis and characterization of $(NH_4)_2(MoO_2S_2)$ and LDH-MoO_2S_2 (XRD, Elemental Mapping, EDS, XPS, EXAFS, UV-Vis absorption Spectra). Details on uptake study as well as characterization of post adsorption LDH-MoO_2S_2.

This information is available free of charge at the website: http://pubs.acs.org/

REFERENCE

(1) Holmes, A. B.; Gu, F. X. Emerging Nanomaterials for the Application of Selenium Removal for Wastewater Treatment. *Environ. Sci. Nano* **2016**, *3* (5), 982–996. https://doi.org/10.1039/C6EN00144K.

(2) Ma, B.; Fernandez-Martinez, A.; Grangeon, S.; Tournassat, C.; Findling, N.; Carrero, S.; Tisserand, D.; Bureau, S.; Elkaïm, E.; Marini, C.; Aquilanti, G.; Koishi, A.; Marty, N. C. M.; Charlet, L. Selenite Uptake by Ca–Al LDH: A Description of Intercalated Anion Coordination Geometries. *Environ. Sci. Technol.* **2018**, *52* (3), 1624–1632. https://doi.org/10.1021/acs.est.7b04644.

(3) Mayordomo, N.; Foerstendorf, H.; Lützenkirchen, J.; Heim, K.; Weiss, S.; Alonso, U.; Missana, T.; Schmeide, K.; Jordan, N. Selenium(IV) Sorption Onto γ-Al2O3: A Consistent Description of the Surface Speciation by Spectroscopy and Thermodynamic Modeling. *Environ. Sci. Technol.* **2018**, *52* (2), 581–588. https://doi.org/10.1021/acs.est.7b04546.
(4) Carrero, S.; Fernandez-Martinez, A.; Pérez-López, R.; Poulain, A.; Salas-Colera, E.; Nieto, J. M. Arsenate and Selenate Scavenging by Basaluminite: Insights into the Reactivity of Aluminum Phases in Acid Mine Drainage. *Environ. Sci. Technol.* **2017**, *51* (1), 28–37. https://doi.org/10.1021/acs.est.6b03315.
(5) Ilgen, A. G.; Kruichak, J. N.; Artyushkova, K.; Newville, M. G.; Sun, C. Redox Transformations of As and Se at the Surfaces of Natural and Synthetic Ferric Nontronites: Role of Structural and Adsorbed Fe(II). *Environ. Sci. Technol.* **2017**, *51* (19), 11105–11114. https://doi.org/10.1021/acs.est.7b03058.
(6) Lee, C.-G.; Kim, S.-B. Removal of Arsenic and Selenium from Aqueous Solutions Using Magnetic Iron Oxide Nanoparticle/Multi-Walled Carbon Nanotube Adsorbents. *Desalination Water Treat.* **2016**, *57* (58), 28323–28339. https://doi.org/10.1080/19443994.2016.1185042.
(7) Li, T.; Xu, H.; Zhang, Y.; Zhang, H.; Hu, X.; Sun, Y.; Gu, X.; Luo, J.; Zhou, D.; Gao, B. Treatment Technologies for Selenium Contaminated Water: A Critical Review. *Environ. Pollut.* **2022**, *299*, 118858. https://doi.org/10.1016/j.envpol.2022.118858.
(8) Lichtfouse, E.; Morin-Crini, N.; Bradu, C.; Boussouga, Y.-A.; Aliaskari, M.; Schäfer, A. I.; Das, S.; Wilson, L. D.; Ike, M.; Inoue, D.; Kuroda, M.; Déon, S.; Fievet, P.; Crini, G. Methods for Selenium Removal from Contaminated Waters: A Review. *Environ. Chem. Lett.* **2022**, *20* (3), 2019–2041. https://doi.org/10.1007/s10311-022-01419-8.
(9) Ullah, H.; Lun, L.; Rashid, A.; Zada, N.; Chen, B.; Shahab, A.; Li, P.; Ali, M. U.; Lin, S.; Wong, M. H. A Critical Analysis of Sources, Pollution, and Remediation of Selenium, an Emerging Contaminant. *Environ. Geochem. Health* **2023**, *45* (5), 1359–1389. https://doi.org/10.1007/s10653-022-01354-1.
(10) Howarth, A. J.; Katz, M. J.; Wang, T. C.; Platero-Prats, A. E.; Chapman, K. W.; Hupp, J. T.; Farha, O. K. High Efficiency Adsorption and Removal of Selenate and Selenite from Water Using Metal-Organic Frameworks. *J. Am. Chem. Soc.* **2015**, *137* (23), 7488–7494. https://doi.org/10.1021/jacs.5b03904.
(11) Hu, B.; Chen, G.; Jin, C.; Hu, J.; Huang, C.; Sheng, J.; Sheng, G.; Ma, J.; Huang, Y. Macroscopic and Spectroscopic Studies of the Enhanced Scavenging of Cr(VI) and Se(VI) from Water by Titanate Nanotube Anchored Nanoscale Zero-Valent Iron. *J. Hazard. Mater.* **2017**, *336*, 214–221. https://doi.org/10.1016/j.jhazmat.2017.04.069.
(12) Xia, X.; Ling, L.; Zhang, W. Solution and Surface Chemistry of the Se(IV)-Fe(0) Reactions: Effect of Initial Solution pH. *Chemosphere* **2017**, *168*, 1597–1603. https://doi.org/10.1016/j.chemosphere.2016.11.150.
(13) Cui, W.; Li, P.; Wang, Z.; Zheng, S.; Zhang, Y. Adsorption Study of Selenium Ions from Aqueous Solutions Using MgO Nanosheets Synthesized by Ultrasonic Method. *J. Hazard. Mater.* **2018**, *341*, 268–276. https://doi.org/10.1016/j.jhazmat.2017.07.073.
(14) Yamani, J. S.; Lounsbury, A. W.; Zimmerman, J. B. Adsorption of Selenite and Selenate by Nanocrystalline Aluminum Oxide, Neat and Impregnated in Chitosan Beads. *Water Res.* **2014**, *50*, 373–381. https://doi.org/10.1016/j.watres.2013.10.054.

(15) Jordan, N.; Müller, K.; Franzen, C.; Brendler, V. Temperature Impact on the Sorption of Selenium(VI) onto Anatase. *J. Colloid Interface Sci.* **2013**, *390* (1), 170–175. https://doi.org/10.1016/j.jcis.2012.09.021.
(16) Xie, W.; Liang, Q.; Qian, T.; Zhao, D. Immobilization of Selenite in Soil and Groundwater Using Stabilized Fe–Mn Binary Oxide Nanoparticles. *Water Res.* **2015**, *70*, 485–494. https://doi.org/10.1016/j.watres.2014.12.028.
(17) Malhotra, M.; Pal, M.; Pal, P. A Response Surface Optimized Nanofiltration-Based System for Efficient Removal of Selenium from Drinking Water. *J. Water Process Eng.* **2020**, *33*, 101007. https://doi.org/10.1016/j.jwpe.2019.101007.
(18) Kalaitzidou, K.; Bakouros, L.; Mitrakas, M. Techno-Economic Evaluation of Iron and Aluminum Coagulants on Se(IV) Removal. *Water* **2020**, *12* (3), 672. https://doi.org/10.3390/w12030672.
(19) Labaran, B. A.; Vohra, M. S. Solar Photocatalytic Removal of Selenite, Selenate, and Selenocyanate Species. *CLEAN – Soil Air Water* **2017**, *45* (10), 1600268. https://doi.org/10.1002/clen.201600268.
(20) Trippe, R. C.; Pilon-Smits, E. A. H. Selenium Transport and Metabolism in Plants: Phytoremediation and Biofortification Implications. *J. Hazard. Mater.* **2021**, *404*, 124178. https://doi.org/10.1016/j.jhazmat.2020.124178.
(21) He, W.; Ai, K.; Ren, X.; Wang, S.; Lu, L. Inorganic Layered Ion-Exchangers for Decontamination of Toxic Metal Ions in Aquatic Systems. *J. Mater. Chem. A* **2017**, *5* (37), 19593–19606. https://doi.org/10.1039/C7TA05076C.
(22) Liao, Z.; He, T.; Shi, L.; Liu, Y.; Zhou, X.; Wang, J.; Li, W.; Zhang, Y.; Wang, H.; Xu, R. Selenium Oxoanions Removal from Wastewater by MoS_4^{2-} Intercalated FeMgAl LDH: Catalytic Roles of Fe and Mechanism Insights. *Catalysts* **2022**, *12* (12), 1592. https://doi.org/10.3390/catal12121592.
(23) Asiabi, H.; Yamini, Y.; Shamsayei, M. Highly Selective and Efficient Removal of Arsenic(V), Chromium(VI) and Selenium(VI) Oxyanions by Layered Double Hydroxide Intercalated with Zwitterionic Glycine. *J. Hazard. Mater.* **2017**, *339*, 239–247. https://doi.org/10.1016/j.jhazmat.2017.06.042.
(24) Celik, A.; Baker, D. R.; Arslan, Z.; Zhu, X.; Blanton, A.; Nie, J.; Yang, S.; Ma, S.; Han, F. X.; Islam, S. M. Highly Efficient, Rapid, and Concurrent Removal of Toxic Heavy Metals by the Novel 2D Hybrid LDH–$[Sn_2S_6]$. *Chem. Eng. J.* **2021**, *426*, 131696. https://doi.org/10.1016/j.cej.2021.131696.
(25) Wang, Y.; Zhang, M.; Liu, Y.; Zheng, Z.; Liu, B.; Chen, M.; Guan, G.; Yan, K. Recent Advances on Transition-Metal-Based Layered Double Hydroxides Nanosheets for Electrocatalytic Energy Conversion. *Adv. Sci.* **2023**, *10* (13), 2207519. https://doi.org/10.1002/advs.202207519.
(26) Mandal, S.; Mayadevi, S.; Kulkarni, B. D. Adsorption of Aqueous Selenite [Se(IV)] Species on Synthetic Layered Double Hydroxide Materials. *Ind. Eng. Chem. Res.* **2009**, *48* (17), 7893–7898. https://doi.org/10.1021/ie900136s.
(27) Ma, L.; Islam, S. M.; Liu, H.; Zhao, J.; Sun, G.; Li, H.; Ma, S.; Kanatzidis, M. G. Selective and Efficient Removal of Toxic Oxoanions of As(III), As(V), and Cr(VI) by Layered Double Hydroxide Intercalated with MoS_4^{2-}. *Chem. Mater.* **2017**, *29* (7), 3274–3284. https://doi.org/10.1021/acs.chemmater.7b00618.

(28) He, Y.; Xiang, Y.; Zhou, Y.; Yang, Y.; Zhang, J.; Huang, H.; Shang, C.; Luo, L.; Gao, J.; Tang, L. Selenium Contamination, Consequences and Remediation Techniques in Water and Soils: A Review. *Environ. Res.* **2018**, *164*, 288–301. https://doi.org/10.1016/j.envres.2018.02.037.
(29) Ma, L.; Islam, S. M.; Xiao, C.; Zhao, J.; Liu, H.; Yuan, M.; Sun, G.; Li, H.; Ma, S.; Kanatzidis, M. G. Rapid Simultaneous Removal of Toxic Anions $[HSeO_3]^-$, $[SeO_3]^{2-}$, and $[SeO_4]^{2-}$, and Metals Hg^{2+}, Cu^{2+}, and Cd^{2+} by MoS_4^{2-} Intercalated Layered Double Hydroxide. *J. Am. Chem. Soc.* **2017**, *139* (36), 12745–12757. https://doi.org/10.1021/jacs.7b07123.
(30) McDonald, J. W.; Friesen, G. D.; Rosenhein, L. D.; Newton, W. E. Syntheses and Characterization of Ammonium and Tetraalkylammonium Thiomolybdates and Thiotungstates. *Inorganica Chim. Acta* **1983**, *72*, 205–210. https://doi.org/10.1016/S0020-1693(00)81720-X.
(31) Ma, S.; Fan, C.; Du, L.; Huang, G.; Yang, X.; Tang, W.; Makita, Y.; Ooi, K. Intercalation of Macrocyclic Crown Ether into Well-Crystallized LDH: Formation of Staging Structure and Secondary Host−Guest Reaction. *Chem. Mater.* **2009**, *21* (15), 3602–3610. https://doi.org/10.1021/cm9007393.
(32) Ma, L.; Wang, Q.; Islam, S. M.; Liu, Y.; Ma, S.; Kanatzidis, M. G. Highly Selective and Efficient Removal of Heavy Metals by Layered Double Hydroxide Intercalated with the MoS_4^{2-} Ion. *J. Am. Chem. Soc.* **2016**, *138* (8), 2858–2866. https://doi.org/10.1021/jacs.6b00110.
(33) Roy, S. C.; Rahman, M. A.; Celik, A.; Wilson, S.; Azmy, A.; Bieber, J.; Spanopoulos, I.; Islam, R.; Zhu, X.; Han, F. X.; Islam, S. M. Efficient Removal of Chromium(VI) Ions by Hexagonal Nanosheets of CoAl-MoS_4 Layered Double Hydroxide. *J. Coord. Chem.* **2022**, *75* (11–14), 1581–1595. https://doi.org/10.1080/00958972.2022.2101103.
(34) Benício, L. P. F.; Eulálio, D.; Guimarães, L. de M.; Pinto, F. G.; Costa, L. M. da; Tronto, J. Layered Double Hydroxides as Hosting Matrices for Storage and Slow Release of Phosphate Analyzed by Stirred-Flow Method. *Mater. Res.* **2018**, *21*, e20171004. https://doi.org/10.1590/1980-5373-MR-2017-1004.
(35) Yu, Z.; Yao, H.; Yang, Y.; Yuan, M.; Li, C.; He, H.; Chan, T.-S.; Yan, D.; Ma, S.; Zapol, P.; Kanatzidis, M. G. MoO_xS_y/Ni_3S_2 Microspheres on Ni Foam as Highly Efficient, Durable Electrocatalysts for Hydrogen Evolution Reaction. *Chem. Mater.* **2022**, *34* (2), 798–808. https://doi.org/10.1021/acs.chemmater.1c03682.
(36) Yang, Y.; Yao, H.; Yu, Z.; Islam, S. M.; He, H.; Yuan, M.; Yue, Y.; Xu, K.; Hao, W.; Sun, G.; Li, H.; Ma, S.; Zapol, P.; Kanatzidis, M. G. Hierarchical Nanoassembly of MoS_2/Co_9S_8 /Ni_3S_2 /Ni as a Highly Efficient Electrocatalyst for Overall Water Splitting in a Wide pH Range. *J. Am. Chem. Soc.* **2019**, *141* (26), 10417–10430. https://doi.org/10.1021/jacs.9b04492.
(37) Cao, J.; Zhou, J.; Zhang, Y.; Wang, Y.; Liu, X. Dominating Role of Aligned MoS_2/Ni_3S_2 Nanoarrays Supported on Three-Dimensional Ni Foam with Hydrophilic Interface for Highly Enhanced Hydrogen Evolution Reaction. *ACS Appl. Mater. Interfaces* **2018**, *10* (2), 1752–1760. https://doi.org/10.1021/acsami.7b16407.
(38) Hou, Y.; Xin, J.; Gómez-García, C. J.; Xiao, B.; Pang, H.; Ma, H.; Wang, X.; Tan, L. A Facile Strategy to Create Electrocatalysts of Highly Dispersive Ni–Mo Sulfide Nanosheets on Graphene by Derivation of Polyoxometalate Coordination Polymer for Advanced H_2

Evolution. *ACS Appl. Energy Mater.* **2021**, *4* (11), 13191–13198. https://doi.org/10.1021/acsaem.1c02800.
(39) Nanda, S.; Asl, H. Y.; Bhargav, A.; Manthiram, A. Thiometallate-Mediated Polysulfide Chemistry and Lithium Stabilization for Stable Anode-Free Lithium-Sulfur Batteries. *Cell Rep. Phys. Sci.* **2022**, *3* (4), 100808. https://doi.org/10.1016/j.xcrp.2022.100808.
(40) Islam, T.; Li, M.; Blanton, A.; Pitton, K. A.; Rao, K. R.; Bayat, S.; Wiaderek, K. M.; Weret, M. A.; Roy, S. C.; Feng, R.; Li, D.; Alam, R.; Nie, J.; Oketola, O.; Pramanik, A.; Guiton, B. S.; Risko, C.; Belharouak, I.; Amin, R.; Islam, S. M. Chalcocarbogels as High-Capacity and Cycle-Stable Electrode Materials for Lithium and Sodium Ion Batteries. *ACS Energy Lett.* **2023**, 1–9. https://doi.org/10.1021/acsenergylett.3c02112.
(41) Blanton, A.; Islam, T.; Roy, S. C.; Celik, A.; Nie, J.; Baker, D. R.; Li, D.; Taylor-Pashow, K.; Zhu, X.; Pramanik, A.; Amin, R.; Feng, R.; Chernikov, R.; Islam, S. M. Porous Semiconducting K–Sn–Mo–S Aerogel: Synthesis, Local Structure, and Ion-Exchange Properties. *Chem. Mater.* **2023**. https://doi.org/10.1021/acs.chemmater.3c01675.
(42) Ma, S.; Shim, Y.; Islam, S. M.; Subrahmanyam, K. S.; Wang, P.; Li, H.; Wang, S.; Yang, X.; Kanatzidis, M. G. Efficient Hg Vapor Capture with Polysulfide Intercalated Layered Double Hydroxides. *Chem. Mater.* **2014**, *26* (17), 5004–5011. https://doi.org/10.1021/cm5020477.
(43) Escalera-López, D.; Lou, Z.; Rees, N. V. Benchmarking the Activity, Stability, and Inherent Electrochemistry of Amorphous Molybdenum Sulfide for Hydrogen Production. *Adv. Energy Mater.* **2019**, *9* (8), 1802614. https://doi.org/10.1002/aenm.201802614.
(44) Liu, Y.; Li, J.; Das, A.; Kim, H.; Jones, L. O.; Ma, Q.; Bedzyk, M. J.; Schatz, G. C.; Kratish, Y.; Marks, T. J. Synthesis and Structure–Activity Characterization of a Single-Site MoO_2 Catalytic Center Anchored on Reduced Graphene Oxide. *J. Am. Chem. Soc.* **2021**, *143* (51), 21532–21540. https://doi.org/10.1021/jacs.1c07236.
(45) Weber, Th.; Muijsers, J. C.; Van Wolput, J. H. M. C.; Verhagen, C. P. J.; Niemantsverdriet, J. W. Basic Reaction Steps in the Sulfidation of Crystalline MoO_3 to MoS_2 , As Studied by X-Ray Photoelectron and Infrared Emission Spectroscopy. *J. Phys. Chem.* **1996**, *100* (33), 14144–14150. https://doi.org/10.1021/jp961204y.
(46) Coucouvanis, D.; Koo, S. M. Rational Synthesis of Monooxo Thioanions from Tetrakis(Benzenethiolato)Oxomolybdate(1-). Structural Characterization of the $[Ph_4P]^+$ Salts of the $[(.Eta._2\text{-}S_2)MoO(.Mu.\text{-}S)_2MoS(.Eta._2\text{-}S_2)]^{2-}$, $[(.Eta._2\text{-}S_2)MoO(MoS_4)]^{2-}$, $[(S_4)MoX(.Mu.\text{-}S)_2MoSX(.Eta._2\text{-}S_2)]^{2-}$ (X = S, O), and $[(S_4)MoO(MoS_4)]^{2-}$ Anions. *Inorg. Chem.* **1989**, *28* (1), 2–5. https://doi.org/10.1021/ic00300a002.
(47) Coucouvanis, D.; Toupadakis, A.; Hadjikyriacou, A. Synthesis of Thiomolybdenyl Complexes with $[Mo_2(S)_2(O)_2]^{2+}$ Cores and Substitutionally Labile Ligands. Crystal and Molecular Structure of the Tris(Dimethylformamide)Dioxotetrasulfidodimolybdenum Complex. *Inorg. Chem.* **1988**, *27* (19), 3272–3273. https://doi.org/10.1021/ic00292a005.
(48) McAllister, J.; Bandeira, N. A. G.; McGlynn, J. C.; Ganin, A. Y.; Song, Y.-F.; Bo, C.; Miras, H. N. Tuning and Mechanistic Insights of Metal Chalcogenide Molecular Catalysts for the Hydrogen-Evolution Reaction. *Nat. Commun.* **2019**, *10* (1), 370. https://doi.org/10.1038/s41467-018-08208-4.
(49) Pless, J. D.; Kim, H.-S.; Smit, J. P.; Wang, X.; Stair, P. C.; Poeppelmeier, K. R. Structure of $Mg_{2.56}V_{1.12}W_{0.88}O_8$ and Vibrational Raman Spectra of $Mg_{2.5}VWO_8$ and $Mg_{2.5}VMoO_8$. *Inorg. Chem.* **2006**, *45* (2), 514–520. https://doi.org/10.1021/ic051740h.

(50) Allen, P. G.; Gash, A. E.; Dorhout, P. K.; Strauss, S. H. XAFS Studies of Soft-Heavy-Metal-Ion-Intercalated M_xMoS_2 ($M = Hg^{2+}$, Ag^{+}) Solids. *Chem. Mater.* **2001**, *13* (7), 2257–2265. https://doi.org/10.1021/cm000389p.
(51) Tran, N. V.; Tieu, A. K.; Zhu, H. First-Principles Molecular Dynamics Study on the Surface Chemistry and Nanotribological Properties of MgAl Layered Double Hydroxides. *Nanoscale* **2021**, *13* (9), 5014–5025. https://doi.org/10.1039/D0NR08706H.
(52) Clegg, W.; Mohan, N.; Mueller, A.; Neumann, A.; Rittner, W.; Sheldrick, G. M. *Crystal and molecular structure of $[N(CH_3)_4]_2[Mo_2O_2S_2(S_2)_2]$: a compound with two S_2^{2-} ligands*. ACS Publications. https://doi.org/10.1021/ic50209a046.
(53) Celik, A.; Li, D.; Quintero, M. A.; Taylor-Pashow, K. M. L.; Zhu, X.; Shakouri, M.; Roy, S. C.; Kanatzidis, M. G.; Arslan, Z.; Blanton, A.; Nie, J.; Ma, S.; Han, F. X.; Islam, S. M. Removal of CrO_4^{2-}, a Nonradioactive Surrogate of $^{99}TcO_4^-$, Using LDH–Mo_3S_{13} Nanosheets. *Environ. Sci. Technol.* **2022**, *56* (12), 8590–8598. https://doi.org/10.1021/acs.est.1c08766.
(54) $Mo_3S_{13}^{2-}$ Intercalated Layered Double Hydroxide: Highly Selective Removal of Heavy Metals and Simultaneous Reduction of Ag^+ Ions to Metallic Ag^0 Ribbons. https://doi.org/10.1002/anie.202112511.
(55) Celik, A.; Roy, S. C.; Quintero, M. A.; Taylor-Pashow, K.; Li, D.; Kanatzidis, M. G.; Zhu, X.; Islam, S. M. Unveiling the Potential of $[Sn_2S_6]^{4-}$ Functionalized Layered Double Hydroxides for the Sorption of ReO_4^- as a Surrogate for $^{99}TcO_4^-$. *ACS Appl. Eng. Mater.* **2023**, *1* (7), 1711–1718. https://doi.org/10.1021/acsaenm.3c00074.
(56) Chen, L.; Xu, H.; Xie, J.; Liu, X.; Yuan, Y.; Liu, P.; Qu, Z.; Yan, N. $[SnS_4]^{4-}$ Clusters Modified MgAl-LDH Composites for Mercury Ions Removal from Acid Wastewater. *Environ. Pollut.* **2019**, *247*, 146–154. https://doi.org/10.1016/j.envpol.2018.12.009.
(57) US EPA, O. *Drinking Water Regulations*. https://www.epa.gov/dwreginfo/drinking-water-regulations (accessed 2023-10-09).
(58) Organization, W. H. *Guidelines for Drinking-Water Quality*; World Health Organization, 2004.
(59) Ma, S.; Huang, L.; Ma, L.; Shim, Y.; Islam, S. M.; Wang, P.; Zhao, L.-D.; Wang, S.; Sun, G.; Yang, X.; Kanatzidis, M. G. Efficient Uranium Capture by Polysulfide/Layered Double Hydroxide Composites. *J. Am. Chem. Soc.* **2015**, *137* (10), 3670–3677. https://doi.org/10.1021/jacs.5b00762.
(60) Manos, M. J.; Ding, N.; Kanatzidis, M. G. Layered Metal Sulfides: Exceptionally Selective Agents for Radioactive Strontium Removal. *Proc. Natl. Acad. Sci.* **2008**, *105* (10), 3696–3699. https://doi.org/10.1073/pnas.0711528105.
(61) Kameda, T.; Kondo, E.; Yoshioka, T. Equilibrium and Kinetic Studies of Se(VI) Removal by Mg–Al Layered Double Hydroxide Doped with Fe^{2+}. *RSC Adv.* **2014**, *4* (106), 61817–61822. https://doi.org/10.1039/C4RA11645C.
(62) Zhu, L.; Zhang, L.; Li, J.; Zhang, D.; Chen, L.; Sheng, D.; Yang, S.; Xiao, C.; Wang, J.; Chai, Z.; Albrecht-Schmitt, T. E.; Wang, S. Selenium Sequestration in a Cationic Layered Rare Earth Hydroxide: A Combined Batch Experiments and EXAFS Investigation. *Environ. Sci. Technol.* **2017**, *51* (15), 8606–8615. https://doi.org/10.1021/acs.est.7b02006.
(63) Lin, W.; Wu, P.; Li, R.; Li, J.; Cai, Y.; Yuan, L.; Feng, W. Novel Triazine-Based Cationic Covalent Organic Polymers for Highly Efficient and Selective Removal of Selenate from

Contaminated Water. *J. Hazard. Mater.* **2022**, *436*, 129127. https://doi.org/10.1016/j.jhazmat.2022.129127.
(64) Cai, H.; Bao, H.; Zhang, X.; Lei, L.; Xiao, C. Highly Efficient Sorption of Selenate and Selenite onto a Cationic Layered Single Hydroxide via Anion Exchange and Inner-Sphere Complexation. *Chem. Eng. J.* **2021**, *420*, 129726. https://doi.org/10.1016/j.cej.2021.129726.
(65) Guo, B.; Liu, H.; Pang, J.; Lyu, Q.; Wang, Y.; Fan, W.; Lu, X.; Sun, D. Tunable Rare-Earth Metal−organic Frameworks for Ultra-High Selenite Capture. *J. Hazard. Mater.* **2022**, *436*, 129094. https://doi.org/10.1016/j.jhazmat.2022.129094.
(66) Tahmasebi, E. Insights into the Adsorption Mechanism of Al30 Polyoxocations-Modified Graphene Oxide Nanosheets for Efficient Removal of Phosphate, Chromate and Selenate Oxyanions: A Comparative Study. *J. Mol. Liq.* **2020**, *299*, 112111. https://doi.org/10.1016/j.molliq.2019.112111.
(67) Sharma, S.; Let, S.; Desai, A. V.; Dutta, S.; Karuppasamy, G.; Shirolkar, M. M.; Babarao, R.; Ghosh, S. K. Rapid, Selective Capture of Toxic Oxo-Anions of Se(IV), Se(VI) and As(V) from Water by an Ionic Metal–Organic Framework (iMOF). *J. Mater. Chem. A* **2021**, *9* (10), 6499–6507. https://doi.org/10.1039/D0TA04898D.
(68) Li, D.; Yan, W.; Guo, X.; Tian, Q.; Xu, Z.; Zhu, L. Removal of Selenium from Caustic Solution by Adsorption with CaAl Layered Double Hydroxides. *Hydrometallurgy* **2020**, *191*, 105231. https://doi.org/10.1016/j.hydromet.2019.105231.
(69) Sun, F.; Zhu, Y.; Liu, X.; Chi, Z. Highly Efficient Removal of Se(IV) Using Reduced Graphene Oxide-Supported Nanoscale Zero-Valent Iron (nZVI/rGO): Selenium Removal Mechanism. *Environ. Sci. Pollut. Res.* **2023**, *30* (10), 27560–27569. https://doi.org/10.1007/s11356-022-24226-8.
(70) Iwakuro, H.; Tatsuyama, C.; Ichimura, S. XPS and AES Studies on the Oxidation of Layered Semiconductor GaSe. *Jpn. J. Appl. Phys.* **1982**, *21* (1R), 94. https://doi.org/10.1143/JJAP.21.94.
(71) Shenasa, M.; Sainkar, S.; Lichtman, D. XPS Study of Some Selected Selenium Compounds. *J. Electron Spectrosc. Relat. Phenom.* **1986**, *40* (4), 329–337. https://doi.org/10.1016/0368-2048(86)80043-3.
(72) Miyake, I.; Tanpo, T.; Tatsuyama, C. XPS Study on the Oxidation of InSe. *Jpn. J. Appl. Phys.* **1984**, *23* (2R), 172. https://doi.org/10.1143/JJAP.23.172.